Implementation of Nanostructured Catalysts in the Electrochemical Promotion of Catalysis

34

Holly A. E. Dole and Elena A. Baranova

Contents

Abstract

In the last 30 years, electrochemical promotion of catalysis (EPOC), also referred to as the non-Faradaic electrochemical modification of catalytic activity (NEMCA), has been extensively studied by research groups due to its ability to considerably enhance catalytic activity of heterogeneous catalysts. Application of a very small electrical stimulus to a catalyst-working electrode results in the modification of its electronic properties due to the controlled in situ addition or removal of the ionic species. Modification of the electronic properties alters the adsorption strength of the reaction components resulting in a distinct change in catalytic performance. Throughout the years, it has been shown that this phenomenon can be applied to various types of reactions, solid electrolytes, and conductive catalysts. Recent studies have been focused on developing these catalytic systems toward a more practical application. One aspect in regard to

H.A.E. Dole • E.A. Baranova (✉)
Department of Chemical and Biological Engineering, and Centre for Catalysis Research and Innovation, University of Ottawa, Ottawa, ON, Canada
e-mail: holly.dole@uottawa.ca; Elena.Baranova@uottawa.ca

M. Aliofkhazraei, A.S.H. Makhlouf (eds.), *Handbook of Nanoelectrochemistry*,
DOI 10.1007/978-3-319-15266-0_29

this includes introducing nanostructured catalysts in the form of nanoparticles or nano-thin films as the working electrode to lower manufacturing costs or with the goal of applying EPOC to commercial highly dispersed catalysts. This involves the synthesis of new nanosized catalysts as well as altering the electrochemical cell design. A review of the current progress (from 2005 up to date) and challenges encountered in EPOC with nanoparticle catalysts using various ionic conducting ceramic and polymer supports will be discussed.

Keywords
Heterogeneous catalysis • Nanoparticles • Metal-support interaction • Electrochemical promotion of catalysis

Introduction

Heterogeneous Catalysis: Nanoparticles, Promotion, and Metal–Support Interaction

The form of catalysis where the reactants are in a different phase as the catalyst itself is referred to as heterogeneous catalysis [1]. The steps carried out during a heterogeneous catalytic reaction are first diffusion of the reactants to the catalyst surface then intraparticle diffusion of the reactants through the catalyst pores to the active sites. The reactants adsorb on the active sites and a surface reaction occurs. The products then desorb from the catalyst sites, intraparticle diffusion of the products occurs, and, finally, there is diffusion of the products away from the catalyst [1].

In heterogeneous catalysis, only the surface atoms are considered active for catalytic reactions; that is, for bulk material, most of the material is not being used (i.e., low volume-to-surface area ratio). The introduction of nanostructured catalysts changed the catalytic ability in heterogeneous catalysis research areas, giving an approach to optimize this volume-to-surface area ratio. To be considered "nano," the catalyst is defined as having at least one dimension in the range of 1–100 nm. There are several methods that have been developed to prepare such nanostructured catalysts. For instance, nanofilms can be prepared through techniques such as physical vapor deposition [2, 3], chemical vapor deposition [4, 5], and atomic layer deposition [6, 7], while nanoparticles can be prepared by impregnation [8–13], deposition–precipitation [8, 14–18], coprecipitation [19–23], sol–gel [24–27], and polyol [28–40] as summarized in Table 1. The nanoparticle catalysts can be supported on two different types of supports, those considered non-active supports (i.e., γ-Al_2O_3, SiO_2, activated carbon) or active (i.e., TiO_2, CeO_2, YSZ, SDC).

An important factor related to the type of support is the dispersion of the catalyst which is defined as the ratio of the number of gas-exposed surface atoms to the total number of catalyst atoms. In general, dispersion increases with decreasing particle size and theoretically approaches 100 % for particles with diameter in the range of 1 nm. It has been shown that, typically, higher dispersion leads to higher catalytic activity due to the presence of more active sites [40, 41–43]. This trend has been

Table 1 Summary of preparation methods for nanoparticles

Method	Synthesized catalyst	Reference
Impregnation	Au/TiO_2	[8]
	Fe_2O_3/SiO_2	[9]
	Ru/SnO_2, Ru/CeO_2, Ru/ZrO_2, $Ru/\gamma\text{-}Al_2O_3$	[10]
	Pt/YSZ	[11, 12]
	Pt–Ir/TiO_2 nanotubes	[13]
Deposition–precipitation	Au/TiO_2	[8]
	$Au/\gamma\text{-}Al_2O_3$	[14]
	Au/TiO_2, Au/CeO_2, Au/Al_2O_3, Au/SiO_2	[15]
	Au–Ag/TiO_2	[16]
	Ag/SiO_2	[17]
	Ag/TiO_2, Au–Ag/TiO_2	[18]
Coprecipitation	Pd-doped CeO_2	[19]
	Fe_3O_4	[20]
	Pd/Al_2O_3	[21]
	$Co_{0.5-x}Mn_xZn_{0.5}Fe_2O_4$	[22]
	$LiFePO_4/C$	[23]
Sol–gel	ZnO, CuO, Cu0.05Zn0.95O	[24]
	$CoFe_2O_4$	[25]
	SnO_2	[26]
	$Ni_{0.7-x}Mg_xCu_{0.3}Fe_2O_4$	[27]
Polyol	Pt	[31]
	Pt	[36–39]
	Ru	[40]
	PtRu	[29]
	PtRu	[34]
	Pt_7Sn_3	[35]
	FePt	[28]
	Ru, Pt	[32, 38]
	Ag	[30]
	Cu	[33]

shown for the same support material (i.e., SiO_2) synthesized with different surface areas [41]. Moreover, the catalytic activity of supported metal or metal oxide nanoparticles can be further enhanced or stabilized by using catalyst promoters or through the metal–support interaction (MSI) phenomenon.

Enhancing the activity of a catalyst through the concept of promotion involves adding a chemical species, referred to as a promoter, during the catalyst preparation procedure to the catalyst in order to change its catalytic behavior. The discovery of this concept was first employed through what is referred to as chemical promotion [44–48]. The addition of such species can result in a change in the electronic and/or crystal structure of the catalyst which improves its catalytic performance, stability, and selectivity for the desired chemical reaction.

Table 2 Summary of the type and use of some electronic promoting species

Promoting species	Catalyst	Reaction	Reference
Potassium (K)	Fe(111), Fe(100)	Adsorption of N_2	[50]
	Ru/ Zeolite-X (Ru–KX)	NH_3synthesis	[51]
	Fe_3O_4(111), α-Fe_2O_3(0001)	Dehydrogenation of ethylbenzene to styrene	[52]
	K–Fe (S6-20) BASF	Dehydrogenation of ethylbenzene to styrene	[53]
Sodium (Na)	Pd/YSZ	NO_x reduction by C_3H_6	[54]
	Pt/γ-Al_2O_3	NO_x reduction by C_3H_6	[55]
	Pt/γ-Al_2O_3	NO_x reduction by C_3H_6 and CO	[56]
	Rh/YSZ	NO_x reduction by CO	[57]
	Pt/YSZ	C_2H_4 oxidation	[58]
Cesium (Cs)	Ru/CsX	NH_3 synthesis	[51]
Cesium (Cs), chlorine (Cl)	Ag_2O	Epoxidation of C_2H_4	[59]
Barium (Ba)	Pt/γ-Al_2O_3	NO_x reduction by C_3H_6	[60]
Magnesium (Mg), barium (Ba)	Ru/BaX, Ru/MgX	NH_3 synthesis	[51]
Magnesium (Mg), barium (Ba), calcium (Ca), strontium (Sr)	Au/Al_2O_3	Partial oxidation of methanol to H_2	[61]
Cobalt (Co), chromium (Cr), molybdenum (Mo)	VPO/TiO_2, VPO/γ-Al_2O_3	Ammoxidation of 2-chloro benzaldehyde to 2-chloro benzonitrile	[62]
Carbon monoxide (CO)	Au(111)	Methanol oxidation	[63]

In general, promoters can be divided into two categories – structural and electronic promoters [46, 49]. Structural promoters (e.g., Al_2O_3) enhance and stabilize the active phase while not participating in the catalytic reaction itself. Contrary to this, electronic promoters (e.g., alkali metal atoms) have a role in the catalytic reaction; they enhance the catalytic properties of the active phase by altering its chemisorptive properties, with respect to bond strength, of the reactants and intermediate species. The focus of this discussion will be on electronic promoters since they are a common factor between chemical and electrochemical promotion, as will be discussed later. Table 2 summarizes some of the different types of electronic promoters and corresponding applications. The most commonly used electronic promoters include potassium [50–53] and sodium [54–58]. Other chemical promoters include other alkali metals (i.e., Cs) [51, 59], alkaline earth metals (i.e., Mg, Ba) [51, 60, 61], and some transition metals (i.e., Co, Cr, Mo) [62].

Potassium, as a chemical promoter, has been used for a variety of chemical reactions and fundamental chemistry studies [50, 51]. A fundamental study was done on a single crystal of Fe(111) and Fe(100) showing a pronounced electron transfer from K to the Fe surfaces; this is attributed to the lowering of the "local" work function near where the potassium atoms are adsorbed [50]. Bécue et al. [51] demonstrated the effect of K promoters on the surface of a zeolite-X-supported Ru catalyst (2 wt%) for the synthesis of ammonia. It was found that the presence of K promoters increases the activity by approximately 70 % for optimal potassium coverage.

For coverage higher than the optimal amount of potassium, it was observed that the activity did not increase; instead, a decrease in activity was attributed to the blocking of active sites due to excess potassium coverage.

More recently, chemical promotion has been shown using other alkali metals such as cesium or alkaline earth metals and transition metals. A recent review on the epoxidation of ethylene to ethylene oxide (EO) over a silver catalyst demonstrated the industrial application of using cesium and chlorine as promoters for the selectivity of EO [59]. It was found that the unpromoted metallic silver catalyst had an EO selectivity around 50 %, while, with the addition of the promoters, the selectivity was enhanced to as high as 90 %. It is proposed that the Cl blocks the nonselective sites and promotes the active oxygen, while Cs acts as a structural promoter. It is said that the Cl promoters weaken the Ag–O bond creating more reactive oxygen to enhance the EO isomerization. On the other hand, Cs interacts with the Ag_2O surface and subsurface oxygen resulting in CsO_x-type complexes.

The use of alkaline earth metals (i.e., Mg, Ca, Sr, Ba) as promoters was shown in one study to enhance both the activity and selectivity of supported gold catalysts (Au/Al_2O_3) in the partial oxidation of methanol to H_2 [61]. It was found that H_2 selectivity increased with increasing basicity of the promoting oxide species (i.e., unpromoted < MgO < CaO < SrO < BaO); however, the opposite trend was observed for the selectivity toward CO and CH_4. Similarly, the effect of transition metal additives on the catalytic properties of a vanadium phosphate (VPO) catalyst was studied for the selective ammoxidation of 2-chloro benzaldehyde to 2-chloro benzonitrile [62]. To observe the effect of such promoters, Co, Mo, and Cr were added to the VPO structure and supported on two different oxide supports – TiO_2 and γ-Al_2O_3. It was observed that a significant improvement in both selectivity and activity existed compared to the bulk VPO catalyst. More specifically, in the case of TiO_2-supported VPO, the addition of Cr exhibited the best performance followed by Mo. From these results, it was also found that the ability of the promoter appears to depend on the nature of the support and its interaction with the catalyst.

Furthermore, traditionally, it has been observed that electropositive species usually promote catalytic reactions, while electronegative species poison the catalyst surface. One electronegative species, CO, has been well known to act as a poison for many metal catalysts; however, recent studies have shown a promotional effect of this species [63, 64]. Rodriguez et al. [63] have demonstrated the promotional effect of adsorbed carbon monoxide for the oxidation of alcohols over a gold catalyst. It was proposed that neighboring adsorbed CO enhances the OH bond on the surface of the catalyst in addition to promoting the breaking of the C–H bond of the alcohol molecules, thus increasing catalytic activity.

A related phenomenon to the promotion of catalytic activity is referred to as metal–support interaction (MSI), where the support plays a key role in changing the properties of the catalyst due the interaction between the two materials, usually resulting in higher catalytic activity [65, 66]. It should be noted that despite the vast amount of MSI studies reported up-to-date, the mechanism and appearance of this effect are still under discussion. Both fundamental and catalytic reaction studies with regard to metal–support interaction are summarized in Table 3.

Table 3 Summary of metal–support interaction studies

Metal catalyst	Support	Reaction	Reference
Ru, Pd, Os, Ir, Pt	TiO_2	H_2, CO sorption	[67]
Pt	YSZ	Not applicable (XPS study)	[39]
Pt	WO_3/C, TiO_2/C, C	Not applicable (XPS study)	[68]
Au	SiO_2, TiO_2	CO oxidation	[41]
Pt	Al_2O_3, TiO_2 (P25, rutile, anatase), CeO_2, SiO_3, MgO	CO oxidation	[43]
PdO	CeO_2, TiO_2, Co_3O_4, Mn_2O_3, SnO_2	CO oxidation	[69]
Pt, Ni	YSZ, γ-Al_2O_3, TiO_2, CeO_2	CO oxidation	[70]
Cu	YSZ, γ-Al_2O_3	CO oxidation	[71–73]
Pt	YSZ, γ-Al_2O_3, C	CO oxidation	[74]
Pt	YSZ, CeO_2, Sm-doped CeO_2, C, γ-Al_2O_3	CO oxidation, C_2H_4 oxidation	[75]
Au	CeO_2/TiO_2	CO oxidation, water–gas shift reaction	[76]
Pd	CeO_2/YSZ	CH_4 oxidation	[77]
Pt	YSZ, RO_2, SiO_2	C_3H_8 oxidation	[12]
Pt	YSZ, γ-Al_2O_3	Toluene oxidation	[78]

Overbury et al. [41] showed that for equally sized Au nanoparticles supported on SiO_2 (lower surface area) and TiO_2 (higher surface area), the catalytic activity was higher for the TiO_2-supported catalysts due to stronger metal–support interaction. Similarly, Kimura et al. [43] demonstrated that for the same loading of metal catalysts deposited on Al_2O_3 and TiO_2, a lower dispersion was obtained for the particles supported on Al_2O_3 compared to TiO_2 indicating aggregation of the metal particles. This was attributed as a stronger metal–support interaction between Pt and TiO_2 compared to Pt and Al_2O_3. It is especially noted that the smaller the nanoparticle, the stronger the interactions are with the support, therefore, increasing the effect of the support used [79].

A more specific term, strong metal–support interaction (SMSI), was first introduced in 1978 to describe the significant change in the chemisorptive properties of group VIII noble metals when they were supported on TiO_2 [67, 80]. It was shown that these metals, both unsupported and supported on common materials such as Al_2O_3, chemisorb one hydrogen atom per metal atom; however, in the case of TiO_2, the ability to chemisorb H_2 was either decreased or disappeared completely. It was suggested that SMSI is due to TiOx migration to the catalyst surface. Among other theories, the possibility of d-orbital overlap between the Ti^{4+} cations and supported metal atoms was suggested [80]. More recently, Lewera et al. [68] carried out a study to further understand the change in electronic properties of nanosized metals when deposited on TiO_2 through the analysis of X-ray photoelectron spectroscopy (XPS) data. Pt nanoparticles with an average size of 2 nm were deposited on a composite of TiO_2/C. A downshift in binding energy of the Pt $4f_{7/2}$ peak was observed which indicated a local charge density change due to the interaction between the

metal and TiO_2. In addition, the presence of an additional (O 1s) peak for the Pt/TiO_2/C spectrum, compared to Pt/C and TiO_2/C, is attributed to oxygen bonded to Ti alloyed with Pt indicating the interaction between the two materials. The analysis of the Ti 2p peak also showed a downshift in binding energy for the supported Pt sample suggesting a new electronic state of Ti.

Similarly, Ntais et al. [39] conducted an XPS study for YSZ-supported Pt nanoparticles which also showed a downshift in the binding energy for smaller Pt nanoparticles indicating a stronger interaction with the support.

Several recent studies have studied the MSI phenomenon, not only using TiO_2-supported metals but employing other ionic and mixed ionic–electronic conducting materials as well. High catalytic activity toward the water–gas shift reactions was shown for a Au/CeO_x/TiO_2(110) catalyst [76]. The high catalytic activity was attributed to the chemical properties of Ce_2O_3, which was formed through the interaction with TiO_2 and its effect at the ceria–gold interfaces. Similarly, Jiménez-Borja et al. [77] demonstrated a strong interaction between Pd and CeO_2 for a Pd/CeO_2/YSZ catalyst for the oxidation of methane. It was observed that the presence of ceria caused a decrease in the size of Pd^0 particles (from 280 to 103 nm) and an increase in the size of PdO particles. This is attributed to the oxygen storage properties of CeO_2 which seems to play a key role in the formation of PdO. Higher catalytic activity was observed for the catalysts containing more PdO compared to Pd. Furthermore, Pd catalysts supported on highly ordered mesoporous metal oxides (i.e., CeO_2, TiO_2, Co_3O_4, Mn_2O_3, and SnO_2) for the oxidation of CO were carried out to demonstrate the interaction between the metal and metal oxide supports [69]. It was found from XPS results that the binding energy of the Pd $3d_{5/2}$ peak for Pd/meso-CeO_2, Pd/meso-SnO_2, and Pd/meso-TiO_2 catalysts shifted more than that for Pd/meso-Co_3O_4 and Pd/meso-Mn_2O_3 indicating that the former catalysts have more surface interactions with the Pd metal. From the catalytic experiments, the bare supports and supported Pd catalysts showed high catalytic activity in the order of $Co_3O_4 > Mn_2O_3 > CeO_2 > SnO_2 > TiO_2$; however, the increase in catalytic activity from bare support to supported Pd catalyst was the highest for the Pd/meso-CeO_2, Pd/meso-SnO_2, and Pd/meso-TiO_2 catalysts indicating the significant role of the support.

Ionically conductive supports or solid electrolytes have immerged as a class of very promising catalyst supports due to their high ionic conductivity, and chemical and mechanical stability [81]. For a material to be ionically conductive, it must possess the structure that allows for either ions to transfer through a series of interstitial sites (i.e., Frenkel defects) or ions to transfer through vacancies in the crystal structure (i.e., Schottky defects) [45, 82, 83]. Some examples include yttria-stabilized zirconia (YSZ) (O^{2-} conductor), K-βAl_2O_3 (K^+ conductor), and Na-$\beta''Al_2O_3$ (Na^+ conductor). As an extension, mixed ionic–electronic materials not only possess ionic conductive capabilities but electronic conductive properties as well [84, 85]. Ion transfer in such materials occurs through structure defects as discussed; however, electronic conductivity occurs through delocalized states in the conduction or valence band, or through localized states by a thermally assisted hopping mechanism. It should be noted that the reason for these properties is independent of each other – ion conductance depends on crystal structure, while electronic conductance

depends on electronic bandgap corresponding to the properties of the constituent ions [84]. Examples of mixed ionic–electronic conducting materials include ceria (CeO_2), titania (TiO_2), and perovskite-type materials in a form of $La_{1-x}A_xCo_{1-y}B_yO_{3-\delta}$ (where A = Sr, Ba, Ca, and B = Fe, Cu, Ni) [85, 86].

Initially, the concept of SMSI was attributed to electronic effect; however, further studies have shown an effect of oxygen vacancies in metal oxides as well. Metcalfe and Sundaresan [70] demonstrated this concept for CO oxidation over Pt and Ni catalysts supported on YSZ, γ-Al_2O_3, TiO_2, and CeO_2. It was found that catalytic activity for the Pt catalysts ranged from $Pt/TiO_2 > Pt/YSZ > Pt/\gamma\text{-}Al_2O_3$. The most interesting results are those for the Ni catalysts where Ni/TiO_2, Ni/YSZ, TiO_2, and YSZ showed significant catalytic activity, with the supported Ni catalyst showing higher activity than their corresponding pure supports. The difference in the activity of Ni/TiO_2 and pure TiO_2 could be attributed to only the electronic effects of TiO_2; however, after observing higher activity for Ni/YSZ compared to pure YSZ, it was proposed that oxygen ion transfer between the metal and support also plays a role in enhancing the catalytic activity. A similar conclusion was found for studies of a copper catalyst supported on γ-Al_2O_3 and YSZ [71–73]. The higher catalytic activity was attributed to the presence of Cu^+ due to the interaction between the copper oxide on the surface of the YSZ and the nearby oxygen vacancies. Vernoux et al. [87] also observed such migration of ionic species from the support to the surface of the nanocatalyst, referring to it as self-induced electrochemical promotion. This concept has been suggested as an explanation for higher catalytic activity for the oxidation of CO over YSZ-supported Pt nanoparticles [36, 74]. It was shown that the catalyst was active for a temperature as low as 40 °C. This high catalytic activity was attributed to the migration of O^{2-} species to the surface which may lead to alterations in the catalytic properties of the Pt nanoparticles. This phenomenon has also been observed for both propane oxidation [87] and toluene oxidation [78] over a Pt/YSZ catalyst. Most recently, Isaifan and Baranova [37, 38, 75] also demonstrated the role of ionic and mixed ionic–electronic supports and the mobility of O^{2-} from these supports for the oxidation of CO and C_2H_4 in an oxygen-free environment. It was found that Pt/YSZ, Pt/CeO_2, and Pt/Sm-doped CeO_2(SDC) have high catalytic activity for CO and C_2H_4 oxidation while Pt/C and $Pt/\gamma\text{-}Al_2O_3$ as well as the blank supports show no catalytic activity in the absence of gaseous O_2. These results imply that O^{2-} from the support reacts with CO and C_2H_4 in an electrochemical reaction at the three phase boundary and the mechanism of nanogalvanic cells was proposed [37].

Electrochemical Promotion of Catalysis

Discovered in the 1980s [88], the phenomenon of electrochemical promotion of catalysis (EPOC), also referred to as non-Faradaic electrochemical modification of catalytic activity (NEMCA), demonstrated a new approach to enhancing the catalytic activity and opened up a new class of promoters previously unknown in heterogeneous catalysis (e.g., O^{2-}, H^+, OH^-, H^+). By applying an electrical current or

potential between the catalyst-working electrode and a counter electrode deposited on a solid electrolyte, it was found that the catalytic activity and selectivity can be significantly altered due to modifications of the electronic properties of the catalyst. Consequently, the adsorption strength of the reaction components is altered resulting in a distinct change in catalytic performance [45]. Compared to chemical promotion, the addition of promoter species is done in situ and can be controlled depending on specified reaction conditions [44, 45, 89–98]. This also implies that promoters with short lifetimes can still effectively be utilized as its coverage on the catalyst surface can be fixed through the application of a current or potential. Therefore, it is said that there is an operational and not a functional difference between chemical and electrochemical promotions [45, 49, 57, 90, 99, 100]. Currently, EPOC has been studied for more than 100 catalytic systems and does not appear to be limited to any specific type of catalytic reaction, metal catalyst, or solid electrolyte. Since the discovery of EPOC, several comprehensive reviews [48, 94, 95, 100–113], book chapters [114–118], and a book [45] have been published to describe this phenomenon; the authors invite the reader to consult these works for comprehensive reading on the EPOC phenomenon. Here, a short overview of the principles, a common experimental setup and reactors, as well as some examples of EPOC with thick, low dispersion film catalysts will be discussed followed by recent studies using nanostructured catalysts.

The concept behind EPOC is that, initially, before current or potential is applied, the catalyst surface is covered by chemisorbed reactants (e.g., O_2 and C_2H_4) in an equilibrated state. Depending on the concentration of the species, there may be more or less of each species adsorbed on the catalyst surface. By applying a current or potential, ions (i.e., O^{2-} in the case of YSZ) from the solid electrolyte either back-spillover (i.e., move to the surface of the catalyst) or spillover (i.e., move from the surface of the catalysts) depending whether the electrochemical cell is positively or negatively polarized, respectively. In the case of back-spillover of the O^{2-} species, it is said that these species form a strong bond on the catalyst surface. The mechanism of this transformation can be seen in the following reaction (Eq. 1) [45]:

$$O^{2-}\left(YSZ\right) \rightarrow \left[O^{\delta-} - \delta +\right]\left(\text{catalyst}\right) + 2e^{-} \tag{1}$$

where $O^{\delta-}$ is the general form of the back-spillover species corresponding to its image charge $\delta+$, indicating that the back-spillover species is overall neutral. The formation of this layer is referred to as an effective double layer. Due to this back-spillover, the oxygen reactant from the gas phase is forced into a weakly bonded state resulting in a more reactive chemisorbed species. Therefore, it is observed that the catalytic rate increases until a new steady-state is reached through the equilibrium of the strongly and weakly bonded oxygen species [45]. The opposite effect is observed for the spillover of the O^{2-} species.

In general, the property of a solid surface that dictates its chemisorptive and catalytic properties is its work function (Φ). By definition, the work function is the minimum energy required for an electron to move from the Fermi level of the solid to an outer point, a few μm outside the surface [45, 119]. Depending on the type of species adsorbed or spilled over onto the catalyst surface, the work function can be

altered accordingly. An electron donor species (e.g., C_2H_4) will cause the work function to decrease, while an electron acceptor species (e.g., O_2) will cause the work function to increase. Four different types of reaction behaviors, in regard to the presence of these species, have been established to classify the relationship between work function and catalytic rate (r) for EPOC studies – electrophobic ($\delta r/\delta\Phi > 0$), electrophilic ($\delta r/\delta\Phi < 0$), volcano type (exhibits a minimum), and inverted volcano type (exhibits a maximum).

More specifically, to evaluate the performance of the catalyst in terms of electrochemical promotion, there are two main parameters that are calculated – rate enhancement ratio (ρ) and Faradaic efficiency (Λ) [45]. The rate enhancement ratio (Eq. 2) is defined as

$$\rho = r / r_0 \tag{2}$$

where r_0 is the open circuit oxidation rate of the reactant species ($\text{mol} \cdot \text{s}^{-1}$) and r is the oxidation rate ($\text{mol} \cdot \text{s}^{-1}$) for an applied current/potential. The Faradaic efficiency (Eq. 3), for an O^{2-} conducting system, is defined as the following:

$$\Lambda = \left(r - r_0\right) / \left(I / 2F\right) \tag{3}$$

where I is the current measured across the cell (A) and F is Faraday's constant (96,485 $\text{C} \cdot \text{mol}^{-1}$). It should be noted that the enhancement is considered to be the effect of electrochemical promotion only when $|\Lambda| > 1$, which indicates non-Faradaic enhancement [45].

First discovered by Comninellis and coworkers [120], another important aspect that is considered in EPOC studies is what is referred to as "permanent" electrochemical promotion of catalysis (P-EPOC). It has been shown that the reversibility of EPOC strongly depends on the duration of polarization and magnitude of applied current or potential. With P-EPOC, after current interruption, the catalytic rate remains higher than the initial open circuit value. In the case of P-EPOC, the permanent rate enhancement can be evaluated using Eq. 4 [120]:

$$\gamma = r_p / r_0 \tag{4}$$

where γ is the permanent rate enhancement ratio and r_p is the catalytic rate ($\text{mol} \cdot \text{s}^{-1}$) at the new steady-state value after current interruption.

Two types of experimental reactors exist to carry out conventional EPOC studies – a fuel cell type reactor and single-chamber type reactor [45]. The fuel cell type reactor (Fig. 1a) consists of two chambers, one in which the catalyst-working electrode is exposed to the reactants and products, while the other chamber contains the counter and reference electrodes which are exposed to a reference gas only. Contrary to this, the single-chamber type reactor (cell configuration in Fig. 1b and typical experimental setup in Fig. 1c) consists of all electrodes exposed to the same reactants and products. The important consideration with this type of reactor is that the reference electrodes must be made of an inert material with respect to the reactants (in most cases, gold is used) to ensure no contribution to the catalytic rate. Conventional EPOC studies were carried out using metal

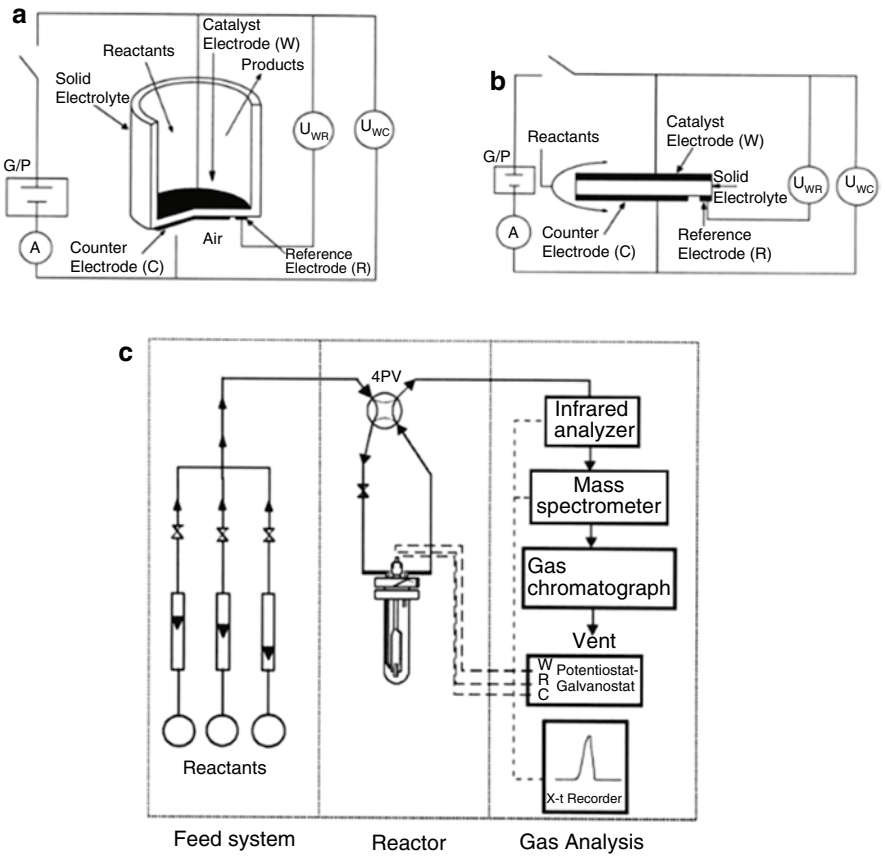

Fig. 1 Schematic of the (**a**) fuel cell type reactor, (**b**) single-chamber type reactor, and (**c**) typical gas flow experimental arrangement using the single-chamber type reactor (Reproduced from Vayenas et al. [45])

(deposited with metallic paste) catalyst films, typically, of a thickness in the range of 5–10 μm [90, 121] and a metal dispersion less than 0.1 % [122]. Typical solid electrolytes include YSZ (O^{2-} conductor), $\beta'Al_2O_3$ (Na^+ conductor), or $\beta''Al_2O_3$ (K^+ conductor).

The EPOC phenomenon has been shown to be effective for various reactions; however, the most common model reaction used in conventional EPOC studies is the complete oxidation of ethylene (Table 4) [88, 90, 94, 121–130]. This was the reaction under observation over a porous Ag film when it was first discovered that pumping and removing oxygen ions from the surface of the catalyst through an applied current can alter the catalytic rate and selectivity [88]. It was then later demonstrated that this effect is not specific to any type of reaction system, although the most significant enhancement (i.e., tenfold increase, Λ up to 15,000) was shown for the oxidation of C_2H_4 over a Pt catalyst [90, 121].

Table 4 Electrochemical promotion of ethylene oxidation for various catalytic systems

Catalyst	Solid electrolyte	Temperature (°C)	Promotion parameters		Reference
			ρ_{max}	$\Lambda_{max/min}$	
Ag	YSZ	320–420	–	<300	[88]
Pt	YSZ	260–420	–	<15,000	[121]
Pt	YSZ	300–450	–	74,000	[90]
Pt	YSZ	375	300	289	[122]
Pt	YSZ	510	–	144	[123]
Rh	YSZ	320–450	1.4	123	[124]
IrO_2	YSZ	380	–	200	[125]
IrO_2	YSZ	380	13	~100	[126]
IrO_2	YSZ	380	2.5	2000	[127]
Pd Pt	YSZ, β″-Al_2O_3 TiO_2	300–400 500	– 21	3000 1880	[128]
Pt	Gd-doped $BaPrO_3$ Y-doped $BaZrO_3$	400–600	1.3	–	[129]
Pt	$La_{0.99}Sr_{0.01}NbO_{4-\delta}$	350–450	1.4	−100	[130]

Enhancement in catalytic activity through this phenomenon for C_2H_4 oxidation has been shown over Pt catalysts supported on YSZ and TiO_2, O^{2-} conducting supports [128]. Further studies for IrO_2 film catalysts supported on YSZ electrolyte showed an enhancement in catalytic activity through an applied positive potential (i.e., oxygen ions migrate to the surface of the catalyst) [125–127]. Permanent promotion was also observed for this system which was attributed to the formation of a higher coordinated oxide at the catalyst/solid interface [126]. Moreover, Koutsodontis et al. [122] demonstrated that the catalyst film thickness for a Pt/YSZ cell is an important factor that affects the magnitude of electrochemical promotion as well, showing that the catalytic rate increases with the increase in film thickness. In addition to O^{2-} conducting electrolytes, positive ion (i.e., Na [128, 131–134], K [135], and H [128–130, 136]) conducting electrolytes have been employed. The electronic effect of these types of promoters are the opposite of that for oxygen ions; that is, by pumping positive ions to the catalyst surface, the work function decreases. In studies involving Na^+ promoters, Na-β″Al_2O_3 is used as a solid electrolyte. In general, it has been found that catalytic activity, for CO [131] or C_2H_4 [128] oxidation and NO reduction by hydrocarbons [132–134], is increased with low Na coverage, while as Na coverage increases, this leads to poisoning of the catalyst surface. Similar observations were found in the case of potassium promoters from a K-β′Al_2O_3 electrolyte for CO oxidation over a Pt catalyst [135]. With regard to the use of H^+ promoters, several different electrolytes have been studied (e.g., Nafion [128, 136], Gd-doped $BaPrO_3$ [129], Y-doped $BaZrO_3$ [129], and $La_{0.99}Sr_{0.01}NbO_{4-\delta}$ [130]). Compared to Na and K, H^+ promoters do not seem to have a significant enhancement of the catalytic activity [129, 130]. In addition to a weak non-Faradaic effect [130].

Although much research has been performed regarding this technology, limitations have been identified that prevent its commercialization. These include eliminating the conventionally used thick film catalysts which have low surface areas and high material costs and moving from theoretical to more practical reactor designs [100]. Overall, the objective is to be able to apply the concept of EPOC to high dispersion heterogeneous catalysts.

Application of Nanostructured Catalysts for EPOC

Highly Dispersed Nanocatalyst Preparation

In heterogeneous catalysis, dispersion of a catalyst has been shown to be an important factor in terms of catalytic performance; the higher the dispersion, the more available the active sites, typically resulting in higher catalytic activity. Dispersion is one aspect of commonly used electrochemical promotion catalysts that has been recognized as an important factor that requires improvement in order to be competitive with the state-of-the-art commercial heterogeneous catalysts. To address the limitation of low metal dispersion found for the catalyst-working electrodes of conventional electrochemical promotion systems, several deposition techniques have been studied (Table 5).

Table 5 Preparation methods of highly dispersed nanocatalysts

Method	Catalyst	Dispersion/loading	Particle size	Film thickness	Reference
Impregnation	Pt	0.2 or higher	–	–	[137]
	Pt	34, 40, 42 %	3.5, 3.0 nm	–	[12]
	Pd	4.9 %	2.6 nm	–	[138]
	Ag	1 %	100 nm	–	[139]
	Ru	3 mg Ru	–	4 μm	[140]
	RuO_2	1.72 g RuO_2/m^2	–	–	[141]
Metal sputtering	Pt	–	40 nm	–	[142,143]
	Pt	–	–	30, 90 nm	[144]
	Pt	2.2, 32 μg Pt/cm^2	–	2, 22 nm	[145]
	Pt	–	–	150 nm	[146]
	Pt	5 %	50 nm	–	[147,148]
	Pt	40 %	–	40 nm	[149]
	Rh	10 %	–	40 nm	[150]
	Rh, Pt	13–40 %	–	40 nm	[151]
	Rh, Pt	>10 %	–	40 nm	[152]
	Rh–Pt	>15 %	–	40 nm	[153]
Electroless deposition	Pd	5 mg Pd	–	–	[155]
Electrostatic spray deposition (ESD)	Pt	250 μg Pt 320 μg Pt 420 μg Pt	9 nm 9 nm 23.2 nm	65 85 110	[156]

The first technique that has been used in recent electrochemical promotion studies that results in near-nanometric or porous films is wet or dry impregnation [137–141]. In general, this type of technique employs a precursor salt of the desired metal dissolved in the solution. The solution is dried on the solid electrolyte, calcined, and reduced in H_2. For example, Marwood and Vayenas [137] dissolved H_2PtCl_6 in water, dried at 80 °C (catalyst 1) and 90 °C (catalyst 2), calcined in air at 450 °C for 1 h, and reduced in 2 % H_2 in helium at 250 °C for 2 h. Using the CO titration technique [157] to determine dispersion, it was found that catalyst 2 had a dispersion of D = 21 % while for catalyst 1, which had a similar mass as catalyst 2 but a surface area of a factor of 5 higher, the dispersion was estimated to be approximately $D \approx 100$ %. A similar procedure was carried out by Jiménez-Borja et al. [138] using a 0.1 M $Pd(NH_3)_4(NO_3)_2$ aqueous solution which resulted in a Pd metal dispersion of 4.9 % for 0.85 mg of Pd deposited. Even though not in the nanometric scale, other groups have demonstrated a decrease in metal required through porous micrometric films, as shown by Theleritis et al. [140] who deposited a porous film of thickness ~4 μm for a loading of approximately 3 mg of catalyst. In addition, Li and Gaillard [139] demonstrated the use of a less expensive metal, Ag, for working electrode films that was of a micrometric thickness of 1.8 and 3.9 μm, and an average crystallite size of approximately 100 nm.

Another common deposition technique that has been employed by many research groups [142–153] to increase catalyst dispersion is metal sputtering, in which the solid electrolyte substrate is placed inside a vacuum chamber in close proximity to the desired metal to be deposited. The desired metal is bombarded with ionized gas molecules in order to displace the metal in small quantities and slowly deposit a thin, nanometric layer on the substrate. This technique has been used by several groups to deposit Rh [150–152], Pt [12, 142–149], or Rh–Pt bimetallic [153] thin-film catalysts. Both Balomenou et al. [151, 152] and Baranova et al. [150, 158, 159] have achieved a film thickness of approximately 40 nm and a dispersion of approximately 13–40 % and 10 %, respectively. Other groups have also shown sputter deposition of Pt that achieves a thickness ranging from 30 to 150 nm, corresponding to dispersions from 5 % to 40 % [142–144, 146–149]. Uniquely, Karoum et al. [145] sputter deposited a thin layer of Pt (~2 nm) on an 80 nm LSM ($La_{0.7}Sr_{0.3}MnO_3$) interlayer where the Pt layer did not necessarily cover the entire surface; however, it was shown to be viable for electrochemical promotion and electronically conductive due to the LSM interlayer. Finally, co-deposition of both Rh and Pt (atomic ratio, 1:1) was performed by Koutsodontis et al. [153] which resulted in an approximate thickness of 40 nm and a total active metal surface area of 1.9×10^{-5} mol metal.

Other research groups have also employed alternative, less common techniques such as electroless deposition [155] and electrostatic spray deposition (ESD) [156]. Lintanf [156] describes the ESD method as using less material compared to conventionally used paste deposition and being fully reproducible. It was reported that three different types of films can be produced – reticulated, dense, and dense – with particles corresponding to film thicknesses of 110, 65, and 85 nm, respectively. The average crystallite size was found to be 23.2 nm for the reticulated film and 9.0 nm for both dense films. Also, an approximate dispersion of 40 % was reported.

Cell Configurations and Reactor Design

Another factor that has been identified and discussed in previous reviews [100, 109] which is preventing commercial application of electrochemical promotion from being achieved is the configuration of the cell and design of the reactor. In a recent comprehensive review, Tsiplakides and Balomenou [100] summarized the considerations taken to address the need for cell configurations that can accommodate thin films and nanoscale catalysts along with designing a more compact reactor that has efficient current collection. The development of electrocatalysts, new configurations such as bipolar or monolithic, and concept of "wireless" EPOC is discussed in this review.

As alluded to in the previous section, the simplest modification to the conventionally used electrochemical promotion cell is to deposit less metal for the working electrode. An important factor to consider, though, is that the metal deposited as a working electrode must remain electronically connected; otherwise, some of the film will not be polarized. Lintanf's [156] description includes a gold mesh on the working electrode side of the cell in order to ensure electronic connectivity for their thin (65–110 nm) Pt catalyst films deposited by ESD. These details are not indicated in other studies [138, 140, 146–148, 160]; however, electrochemical promotion using the conventional cell configuration was observed for catalyst films exhibiting dispersions ranging from 5 % to 80 % demonstrating the presence of at least some electrical connectivity. Similarly, another approach to establish electrical connectivity involves introducing a mixed ionic–electronic conductive (MIEC) interlayer between the nanostructured catalyst and solid electrolyte. Some examples of MIEC interlayer materials that have been used in recent studies include TiO_2 [144, 150, 159], LSM ($La_{0.7}Sr_{0.3}MnO_3$) [145], CeO_2 [161], and LSCF/GDC ($La_{0.6}Sr_{0.4}Co_{0.2}Fe_{0.8}O_{3-\delta}/Ce_{0.9}Gd_{0.1}O_{1.95}$) composite (30 % GDC) [162]. Several methods were used to introduce these interlayers. Baranova et al. [150, 159] deposit TiO_2 (~5 μm thickness) on a YSZ pellet by applying a solution of 20 % TiO_2 in EtOH:H_2O (1:1), evaporating at 60 °C for 10 min, and thermal treatment at 450 °C for 30 min in air; following this deposition, Rh is sputter deposited overlaying the TiO_2. Alternatively, another study showed the use of sputter depositing for both the TiO_2 interlayers (~90 nm thickness) along with the deposition of Pt (~30 nm thickness) [144]. Figure 2 shows SEM micrographs of the deposited layers on the YSZ pellet. It was noted that the YSZ pellet is not fully covered by the TiO_2 interlayer (Fig. 2b).

Both interlayer (LSM) and Pt catalyst were also sputter deposited in a study performed by Karoum et al. [145]; however, interesting to note, the use of a CGO ($Ce_{0.9}Gd_{0.1}O_{2-\delta}$) pellet was shown to be an alternative to using YSZ. For a temperature range of 200–400 °C, the ionic conductivity of the CGO pellet was shown to be at least 10 times higher than that of the YSZ pellet. Finally, as described by Kambolis et al. [162], the electronic conductivity of the catalyst electrode in their EPOC cell was not ensured by the impregnated Pt nanoparticles but by the MIEC interlayer of LSCF/GDC which was deposited through screen printing on a GDC pellet.

The first step toward a modified cell configuration is shown in Fig. 3, proposed by Marwood [163] in the 1990s, in which the catalyst is not used as an electrode as in the conventional EPOC, but rather it is instead electronically isolated with current

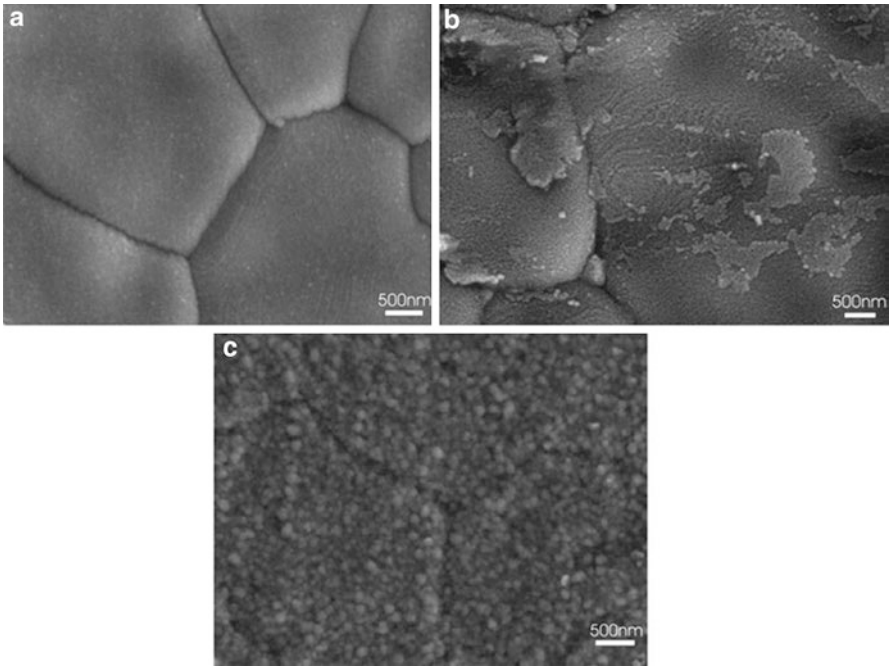

Fig. 2 SEM micrographs of (**a**) YSZ surface, (**b**) sputter-deposited TiO_2 on YSZ surface, and (**c**) sputter-deposited Pt on TiO_2/YSZ surface (Reproduced from Papaioannou et al. [144])

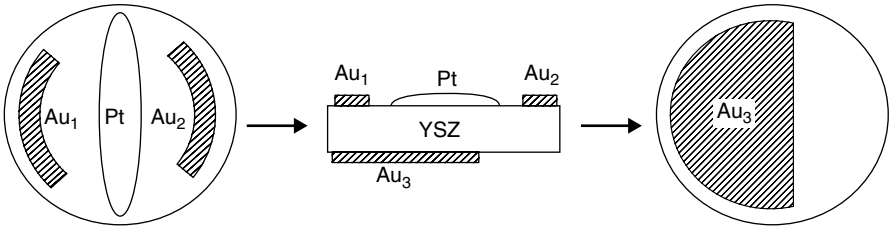

Fig. 3 Schematic of first proposed bipolar configuration, Pt catalyst and Au working (Au_1), counter (Au_2), and reference (Au_3) electrodes (Reproduced from Marwood [163])

passing between two gold electrodes. This pioneering work showed that Pt was deposited using the commonly used paste to determine whether a direct electrical connection between the catalyst and counter electrode was necessary to observe the effect of electrochemical promotion [163].

Similarly, a preceding study demonstrated the use of highly dispersed impregnated Pt (~5 nm) nanoparticles [137]; however, they were deposited on a gold working electrode. From this study, it was shown that direct contact between the catalyst and the solid electrolyte was not necessary as well. In addition, it was also not necessary for the catalyst to be continuous to observe the effects of electrochemical promotion.

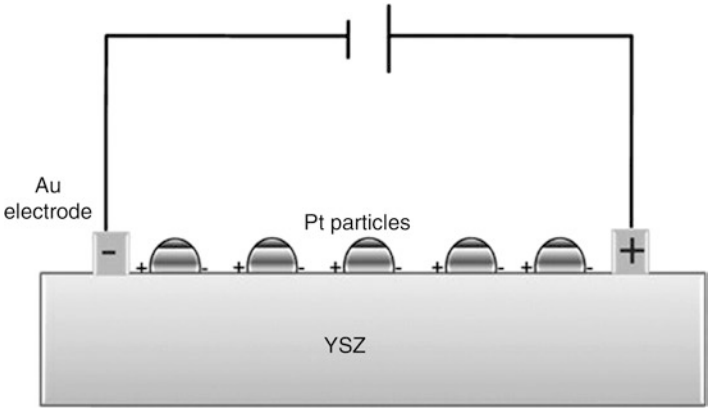

Fig. 4 Schematic of bipolar configuration of electrochemical cell, consisting of two Au electrodes and polarized Pt particles deposited on YSZ solid electrolyte (Reproduced from Xia et al. [143])

Various other cell designs have been proposed and tested by other research groups which fall under the bipolar configuration category. These include depositing Pt metal paste in the forms of stripes or dots between two gold electrodes [164], coating glass beads with Rh and placing them inside a YSZ tube that is coated with two gold electrodes on the outer surface [99], and sputtering Pt between the comb-like gold electrode structures (distance of 2 mm between electrodes) [142]. Figure 4 depicts a bipolar cell configuration presented by Xia et al. [143]. As shown in the figure, it was proposed that upon application of an electrical field, the dispersed Pt nanoparticles form partially or completely polarized galvanic cells, one side being positively polarized and the other negatively polarized.

Further cell modifications were first proposed by Wodiunig et al. [141] through the use of a cylindrical YSZ solid electrolyte monolith. A RuO_2 catalyst was deposited through thermal decomposition (i.e., impregnation) inside the channels of the monolith, while two gold electrodes were deposited symmetrically on the outside of the cylinder. A similar honeycomb monolith was used in a previous study where dispersed Pd particles were introduced into the channels by electroless deposition; however, instead of both electrodes deposited on the outside of the cylinder, a gold working electrode was deposited on the entire outside surface, while a continuous Pd film was deposited (as a counter electrode) on the center channel of the monolith [154]. Furthermore, using this concept of a monolithic reactor and in regard to both the desire for efficient current collection and a compact reactor design, the monolithic electrochemically promoted reactor (MEPR) was proposed by Balomenou et al. [151, 152]. Details of the design and construction of this reactor are well outlined, describing that the main advantage is that it can be assembled and dismantled easily and the plates can be replaced as necessary [151]. This type of reactor has also been employed by Koutsodontis et al. [153] who describe the design as a hybrid between the classical honeycomb monolith and a flat- or ribbed-plate solid oxide fuel cell; a feasible solution in order to minimize electrical connections.

More recently, as modified from the reactor in Fig. 1c, a single-chamber reactor (SCCR) was developed to accomodate highly-dispersed nanocatalysts [155].

A more recent concept that has been related to the electrochemical promotion phenomenon is that of self-induced electrochemical promotion. One of the main advantages of this type of catalytic cell is that there is no electrical contacts required which, in turn, means no external circuit. It has also been a suggestion in order to overcome the limitation of the electrical connectivity of nanocatalysts. This concept has been demonstrated for the oxidation of CO over YSZ-supported Pt nanoparticles [36, 74] as well as for propane oxidation [87] and toluene oxidation [78] over a Pt/YSZ catalyst.

Similarly, the concept of a wireless configuration has been studied as well which involves a concentration driving force that causes the migration of promoting ion species from the support toward the surface of the nanostructured catalyst [165–167]. These studies were also performed for a Pt catalyst deposited on a MIEC support (or membrane). The cell is placed inside a dual chamber reactor which consists of a reaction side (i.e., catalyst, reaction gases) and a sweep side (i.e., catalyst, sweep gas). In this case, open circuit conditions correspond to using the same reaction mixture on each side. To induce back-spillover (i.e., pushing oxygen toward the surface of the reaction side catalyst), oxygen was introduced on the sweep side. This creates an oxygen chemical potential difference across the membrane driving the oxygen toward the reaction side. Furthermore, spillover (i.e., removing oxygen from the surface of the reaction side catalyst) was induced by sweeping hydrogen on the sweep side creating a driving force in the opposite direction [165–167]. It should be noted that the same in situ control of catalytic activity as EPOC can be achieved with this type of wireless configuration by altering the oxygen concentration difference across the membrane.

Electrochemical Promotion of Nanostructured Catalysts

Several model reactions have been used to evaluate and investigate the viability of electrochemical promotion for the nanocatalyst systems (as shown in Table 6). These include complete oxidation of ethylene [40, 141, 144, 150, 151, 158, 159, 163, 164] and propane [12, 145, 146, 148, 162], combustion of CO [142, 143, 147] and natural gas [138, 154, 161], reduction of NO in the presence of hydrocarbons [99, 152, 153, 156, 160], and, more uniquely, SO_2 oxidation [149] and the reverse water–gas shift (RWGS) reaction [140]. Each study has shown promising results for electrochemical promotion over nanocatalysts for different cell configurations and reactor designs which prove to be furthering this technology toward commercialization.

In general, it has been concluded that the reaction rate of ethylene oxidation is significantly increased when a positive polarization is applied [141, 144, 150, 151, 158, 159, 163, 164]; however, a recent study showed an increase in catalytic rate when negative polarization is applied. This was attributed to partial reduction of CeO_2, the catalyst support, causing a stronger MSI of the Ru nanoparticles and CeO_2 [40]. The introduction of a MIEC interlayer, especially TiO_2, was shown to

Table 6 Electrochemical promotion of nanocatalytic systems

Reaction	Catalyst	Solid electrolyte	Temperature (°C)	Promotion parameters		Reference
				ρ_{max}	$\Lambda_{max/min}$	
C_2H_4 oxidation	Pt	YSZ	353	1.38	688	[163]
	Pt	YSZ	400	3.8	–	[164]
	Pt	YSZ TiO_2/YSZ	280	67 168	188 753	[144]
	Pt, Rh	YSZ	300–380	1.45	77	[151]
	Rh	YSZ TiO_2/YSZ	300–420	60 78	1400 1791	[150,158,159]
	Ru	YSZ	350–400	2.46	96	[40]
	RuO_2	YSZ	360	–	90	[141]
C_3H_8 oxidation	Pt	YSZ	350	5.6	330	[146]
	Pt	YSZ	150–500	22.4	480	[148]
	Pt	$Ce_{0.9}Gd_{0.1}O_{2-\delta}$	170–250	1.3	6	[145]
	Pt	$Ce_{0.9}Gd_{0.1}O_{0.95}$	267–338	1.38	85	[161]
CO oxidation	Pt	YSZ	300	500	1.5	[142,143]
	Pt	YSZ	250	4	530	[147]
CH_4 oxidation	Pd	YSZ	400	–	47	[130]
	Pd	YSZ	120–500	3.65	–	[138]
	Pd	CeO_2/YSZ	480	5.6	764	[160]
NO_x reduction	Pt	YSZ	300–510	2.3	48	[156]
	Pt, Rh	YSZ	290–305	14	900	[152]
	Pt–Rh	YSZ	335–380	6.46	13.75	[153]
	Rh	YSZ	275–450	6	5	[99]
	Rh	YSZ	370	220	1207	[160]
SO oxidation	Pt	YSZ	330–370	2	30	[149]
RWGS	Ru	YSZ	200–300	2.5	1000	[140]

enhance the catalytic activity even more [144, 150]. Baranova et al. [150] discuss that this enhancement due to the addition of the TiO_2 interlayer is attributed to the higher surface area of the catalyst deposited on TiO_2 compared to the catalyst deposited on the bare YSZ pellet. Further explanation of this behavior outlines that the TiO_2 layer, under polarization, acts as a catalyst in transforming the gaseous O_2 to promoter O^{2-} species at the Pt/gas interface [144]. Figure 5 shows a comparison of the catalytic performance of the Pt catalyst with and without the incorporation of a TiO_2 interlayer. Some of the observations discussed from these results include that there is an increase in U_{WR} for the Pt/TiO_2/YSZ catalyst which implies an increase in work function indicating a higher coverage of promoting O^{2-} species on the catalyst surface resulting in greater enhancement in activity; also, a new steady state, upon positive polarization, was achieved significantly faster for the Pt/TiO_2/YSZ catalyst compared to the Pt/YSZ catalyst.

Similar results were found using the bipolar configuration by both Marwood [163] and Balomenou et al. [164]; however, it was observed that the magnitude

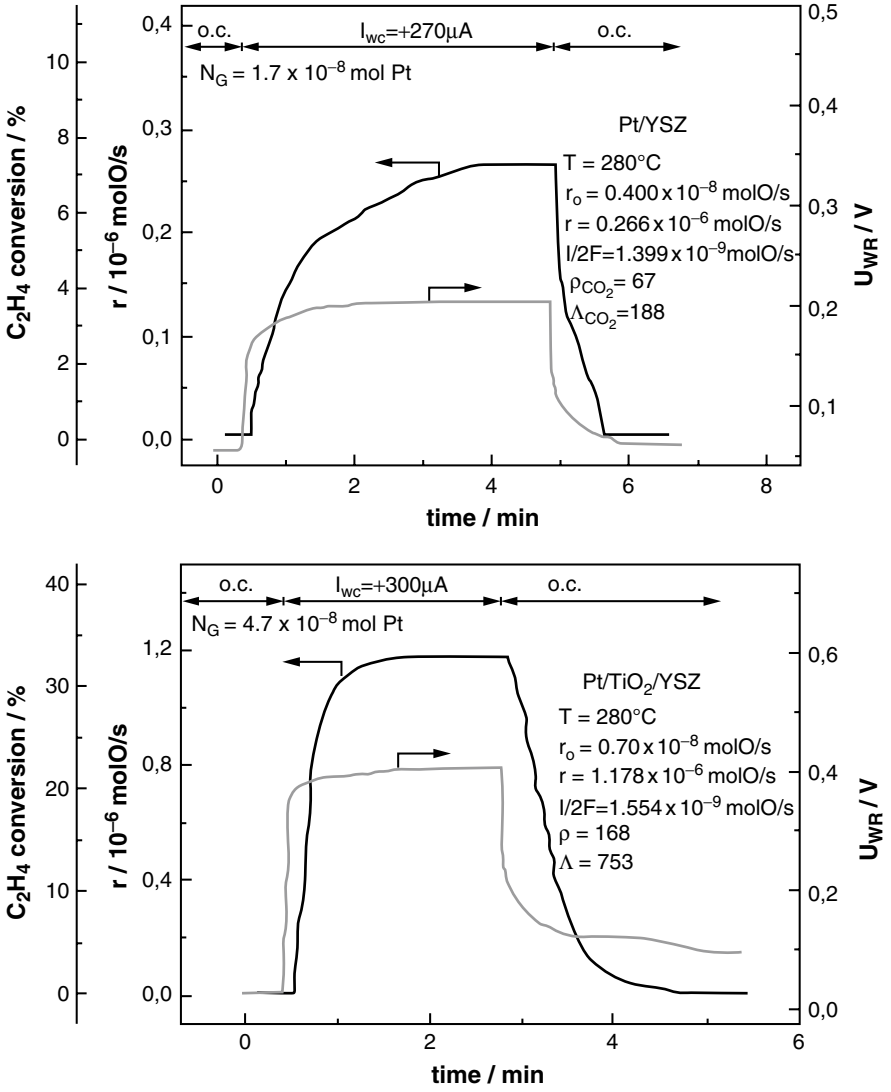

Fig. 5 Transient effect of applied constant current on the rate of C_2H_4 oxidation: (*top*) Pt/YSZ catalyst, (*bottom*) Pt/TiO_2/YSZ catalyst (Reproduced from Papaioannou et al. [144])

of electrochemical promotion (in terms of rate enhancement ratio and Faradaic efficiency) was factors lower than that observed for the conventional configuration. Both groups attributed this to two effects, current bypass and individual bipolar electrodes. Current bypass involves the possibility of current passing through the bulk of the YSZ without affecting the Pt catalyst. Some possible solutions in order to obtain similar catalytic performance include applying much larger currents, or using a thinner YSZ pellet or appropriate electrode geometry to lessen the loss of

current. The concept of individual bipolar electrodes means that each individual Pt nanoparticle catalyst behaves as a bipolar electrode; one side is positively charged, and the other side is negatively charged. This causes a nonuniform work function, contrary to that of a conventional electrode configuration; therefore, the resulting effect is a combination of catalytic activity due to both positive and negative polarizations. It has been suggested that this can be overcome by using this type of configuration for reactions that exhibit both electrophobic and electrophilic behavior.

A similar limitation (i.e., underestimation of promotion parameters) was found by Kambolis et al. [162] for the oxidation of propane over Pt/LSCF-GDC/GDC catalyst. It was stated that a minor part of the applied current between the LSCF/GDC electrode and the counter electrode passes over the Pt nanoparticles resulting in an underestimation of the Faradaic efficiency values. These results are shown in Fig. 6, summarizing the effect of positive polarization at three different temperatures. It can be seen that at 267 °C, a two-step increase of propane conversion was observed. This was attributed to the fact that the LSCF/GDC electrode conductivity is quite low at such a temperature indicating that the movement of oxygen ions requires some time to be delocalized from the bulk of the electrode; the opposite is observed when the current is interrupted [162].

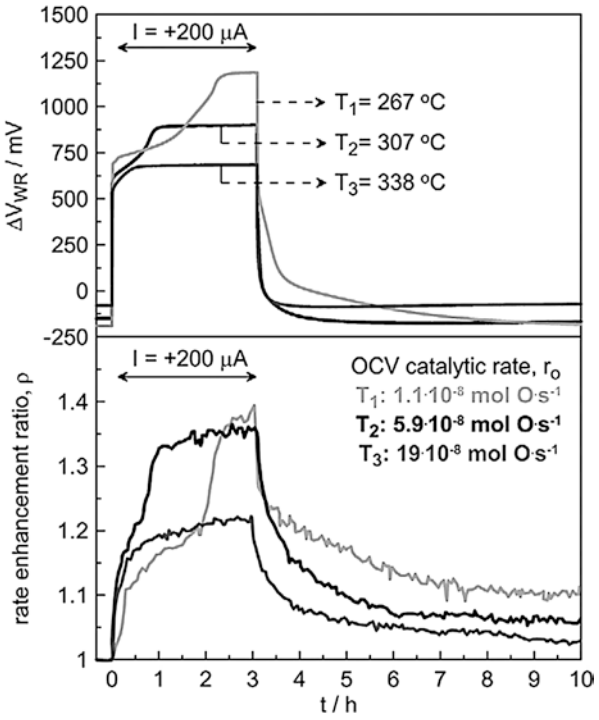

Fig. 6 Transient effect of applied constant current on the rate of C_3H_8 oxidation for T_1, 267 °C; T_2, 307 °C; and T_3, 338 °C (Reproduced from Kambolis et al. [162])

Xia et al. have attempted to quantify this difference in promotion parameters compared to the conventional equations, taking into account that when the catalyst is highly dispersed and not directly electronically connected, it acts as individual, isolated galvanic cells during polarization [143]. They proposed a new technique where a galvanostatic step is applied to a system in the presence of $C^{16}O$ and isotope $^{18}O_2$ under high vacuum conditions. The formation of $C^{18}O_2$ (Faradaic reaction; ^{16}O from YSZ) and $C^{16}O^{18}O$ (non-Faradaic reaction; ^{18}O from $^{18}O_2$) is observed, and the number of galvanic cells is quantified, thus, resulting in the following modified equation (Eq. 5) for rate enhancement ratio being proposed:

$$\rho = \frac{r_{C^{16}O_2} + r_{C^{16}O^{18}O}}{r^0_{C^{16}O^{18}O}} \tag{5}$$

where $r_{C^{16}O_2}$ is the rate of Faradaic formation of $C^{16}O_2$, $r_{C^{16}O^{18}O}$ is the rate of non-Faradaic formation of $C^{16}O^{18}O$, and $r^0_{C^{16}O^{18}O}$ is the initial open circuit catalytic rate. In addition, an adjustment to the equation (Eq. 6) for Faradaic efficiency was shown to be

$$\Lambda = \frac{r_{C^{16}O_2} + \Delta r_{C^{16}O^{18}O}}{r_{C^{16}O_2}} \tag{6}$$

or in the more conventional form (Eq. 7); however, accounting for the equivalent number of galvanic cells (n_{cell}),

$$\Lambda = \frac{2F}{I \cdot n_{cell}} \left(r_{C^{16}O_2} + \Delta r_{C^{16}O^{18}O} \right) \tag{7}$$

where $\Delta r_{C^{16}O^{18}O}$ is the enhancement of the catalytic rate of $C^{16}O^{18}O$ during polarization.

From this discussion, it is evident that some limitations still exist with regard to the application of nanostructured catalysts and the corresponding modified cell configurations and reactor designs; however, these have been identified and are being investigated for possible solutions and explanations. Further fundamental research with regard to these new designs would prove to be beneficial in the understanding of the behavior of these nanostructured catalysts compared to the commonly known systems. In addition, adjusting the reaction environment to more practical operation conditions would make it possible to evaluate the nanostructured catalysts for commercial applications.

Conclusion

Recent progress in the implementation of nanostructured catalysts to overcome the commercial limitations of conventional electrochemical promotion systems and to gain a better understanding of the related MSI phenomenon was presented. The limitations for practical application include the low metal dispersion, high metal

loading of expensive metals, and inefficient cell configuration and reactor design. It was shown that metal dispersion can be increased (by a factor of 10–100) through catalyst preparation techniques such as impregnation, sputter depositing, electroless deposition, and electrostatics spray deposition. In addition, adjustments to the cell configuration to accommodate these nanostructured catalysts, such as using the bipolar configuration or incorporating a mixed ionic–electronic conducting interlayer, have been studied along with new reactor designs, such as the monolithic electrochemical promotion reactor. These modifications have been shown to be the potential solutions to progressing toward commercial applications of electrochemical promotion. However, some of the limitations identified for these new designs include current bypass and individual bipolar electrodes, which cause an underestimation of conventional promotion parameters.

References

1. Dumesic JA, Huber GW, Boudart M (2008) Introduction. In: Ertl G (ed) Handbook of heterogenous catalysis, 2nd edn. Wiley-VCH, Weinheim/Chichester, pp 1–15
2. Mattox DM (1998) Introduction. In: Handbook of physical vapor deposition, Film formation, adhesion, surface preparation and contamination control. Noyes Publications, Westwood, pp 29–55
3. Fee M, Ntais S, Weck A, Baranova EA (2014) Electrochemical behavior of silver thin films interfaced with yttria-stabilized zirconia. J Solid State Electrochem 18:2267–2277
4. Junes AC, Hitchman ML (2009) Chapter 1 Overview of Chemical Deposition Vapor Deposition In: Chemical vapour deposition precursors, processes and applications. Royal Society of Chemistry, Cambridge, UK, pp 1–36
5. Oh T, Haile SM (2015) Electrochemical behavor of thin-film Sm-doped ceria: insights from the point-contact configuration. Phys Chem Chem Phys 17:13501–13511
6. Pinna N, Knez M (2011) Atomic lay deposition of nanostructured materials. Wiley-VCH Verlag & Co, Weinheim, Germany
7. Mamun MA, Gu D, Baumgart H, Elmustafa AA (2015) Nanomechanical properties of platinum thin films synthesized by atomic layer deposition. Sur Coat Tech 265:185–190
8. Li W, Comotti M, Schuth F (2006) Highly reproducible syntheses of active Au/TiO_2 catalysts for CO oxidation by deposition–precipitation or impregnation. J Catal 237:190–196
9. Alcala M, Real C (2006) Synthesis based on the wet impregnation method and characterization of iron and iron oxide-silica nanocomposites. Solid State Ion 177:955–960
10. Mitsui T, Tsutsui K, Matsui T et al (2008) Support effect on complete oxidation of volatile organic compounds over Ru catalysts. Appl Catal B Environ 81:56–63
11. Fortunato MA, Aubert D, Capdeillayre C et al (2011) Dispersion measurement of platinum supported on yttria-stabilised zirconia by pulse H2 chemisorption. Appl Catal A Gen 403:18–24
12. Fortunateo MA, Princivalle A, Capdeillayre et al (2014) Role of Lattice Oxygen in the Propane Combustion Over Pt/Yttria-Stabilized Zirconia: Isotopic Studies. Top Catal 57:1277–1286
13. Toledo-Antonio JA, Ángeles-Chávez C, Cortés-Jácome MA et al (2012) Highly dispersed Pt–Ir nanoparticles on titania nanotubes. Appl Catal A Gen 437–438:155–165
14. Radnik J, Wilde L, Schneider M et al (2006) Influence of the precipitation agent in the deposition-precipitation on the formation and properties of Au nanoparticles supported on Al_2O_3. J Phys Chem B 110:23688–23693
15. Sandoval A, Gómez-Cortés A, Zanella R et al (2007) Gold nanoparticles: support effects for the WGS reaction. J Mol Catal A Chem 278:200–208

16. Sandoval A, Aguilar A, Louis C et al (2011) Bimetallic Au–Ag/TiO_2 catalyst prepared by deposition–precipitation: high activity and stability in CO oxidation. J Catal 281:40–49
17. Qian K, Luo L, Bao H et al (2013) Catalytically active structures of SiO_2-supported Au nanoparticles in low-temperature CO oxidation. Catal Sci Technol 3:679–687
18. Bokhimi X, Zanella R, Maturano V, Morales A (2013) Nanocrystalline Ag, and Au–Ag alloys supported on titania for CO oxidation reaction. Mater Chem Phys 138:490–499
19. Liang H, Raitano JM, He G et al (2011) Aqueous co-precipitation of Pd-doped cerium oxide nanoparticles: chemistry, structure, and particle growth. J Mater Sci 47:299–307
20. Petcharoen K, Sirivat A (2012) Synthesis and characterization of magnetite nanoparticles via the chemical co-precipitation method. Mater Sci Eng B 177:421–427
21. Kumar AP, Kumar BP, Kumar ABVK et al (2013) Preparation of palladium nanoparticles on alumina surface by chemical co-precipitation method and catalytic applications. Appl Surf Sci 265:500–509
22. Sharifi I, Shokrollahi H (2013) Structural, magnetic and mössbauer evaluation of Mn substituted Co–Zn ferrite nanoparticles synthesized by co-precipitation. J Magn Magn Mater 334:36–40
23. Wang S, Yang H, Feng L et al (2013) A simple and inexpensive synthesis route for $LiFePO_4$/C nanoparticles by co-precipitation. J Power Sources 233:43–46
24. Fernandes DM, Silva R, Hechenleitner AAW et al (2009) Synthesis and characterization of ZnO, CuO and a mixed Zn and Cu oxide. Mater Chem Phys 115:110–115
25. Gopalan EV, Joy PA, Al-Omari IA et al (2009) On the structural, magnetic and electrical properties of sol–gel derived nanosized cobalt ferrite. J Alloys Compd 485:711–717
26. Aziz M, Saber Abbas S, Wan Baharom WR (2013) Size-controlled synthesis of SnO_2 nanoparticles by sol–gel method. Mater Lett 91:31–34
27. Batoo KM, El-sadek M-SA (2013) Electrical and magnetic transport properties of Ni–Cu–Mg ferrite nanoparticles prepared by sol–gel method. J Alloys Compd 566:112–119
28. Liu C, Wu X, Klemmer T et al (2004) Polyol process synthesis of monodispersed FePt nanoparticles. J Phys Chem B 108:6121–6123
29. Bock C, Paquet C, Couillard M et al (2004) Size-selected synthesis of PtRu nano-catalysts: reaction and size control mechanism. J Am Chem Soc 126:8028–8037
30. Wiley B, Herricks T, Sun Y, Xia Y (2004) Polyol synthesis of silver nanoparticles: use of chloride and oxygen to promote the formation of single-crystal, truncated cubes and tetrahedrons. Nano Lett 4:1733–1739
31. Herricks T, Chen J, Xia Y (2004) Polyol synthesis of platinum nanoparticles: control of morphology with sodium nitrate. Nano Lett 4:2367–2371
32. Baranova EA, Bock C, Ilin D et al (2006) Infrared spectroscopy on size-controlled synthesized Pt-based nano-catalysts. Surf Sci 600:3502–3511
33. Park BK, Jeong S, Kim D et al (2007) Synthesis and size control of monodisperse copper nanoparticles by polyol method. J Colloid Interface Sci 311:417–424
34. Baranova EA, Le Page Y, Ilin D et al (2009) Size and composition for 1–5nm Ø PtRu alloy nano-particles from Cu Kα X-ray patterns. J Alloys Compd 471:387–394
35. Baranova EA, Amir T, Mercier PHJ et al (2010) Single-step polyol synthesis of alloy Pt_7Sn_3 versus bi-phase Pt/SnO_x nano-catalysts of controlled size for ethanol electro-oxidation. J Appl Electrochem 40:1767–1777
36. Isaifan RJ, Dole HAE, Obeid E et al (2011) Catalytic CO oxidation over Pt nanoparticles prepared from the polyol reduction method supported on yttria-stabilized zirconia. Electrocatal 5, ECS Trans 35:43–57
37. Isaifan RJ, Ntais S, Coulliard M, Baranova EA (2015) Size-dependent activity of Pt/yttria-stabilized zirconia catalyst for ethylene and carbon monoxide oxidation in oxygen-free gas environment. J Catal 324:32–40
38. Isaifan RJ, Baranova EA (2015) Effect of ionically conductive supports on the catalytic activity of platinum and ruthenium nanoparticles for ethylene complete oxidation. Catal Today 241:107–113
39. Ntais S, Isaifan RJ, Baranova EA (2014) An x-ray photoelectron spectroscopy study of platinum nanoparticles on yttria-stabilized zirconia ionic support: Insight into metal support interaction. Mat Chem Phys 148:673–679

40. Dole HAE, Safady LF, Ntais S et al (2014) Electrochemically enhanced metal-support interaction of highly-dispersed Ru nanoparticles with a CeO_2 support. J Catal 318:85–94
41. Overbury SH, Ortiz-soto L, Zhu H et al (2004) Comparison of Au catalysts supported on mesoporous titania and silica: investigation of Au particle size effects and metal-support interactions. Catal Lett 95:99–106
42. Wang Z, Li B, Chen M et al (2010) Size and support effects for CO oxidation on supported Pd catalysts. Sci China Chem 53:2047–2056
43. Kimura K, Einaga H, Teraoka Y (2011) Preparation of highly dispersed platinum catalysts on various oxides by using polymer-protected nanoparticles. Catal Today 164:88–91
44. Vayenas CG, Bebelis S, Ladas S (1990) Dependence of catalytic rates on catalyst work function. Nature 343:625–627
45. Vayenas CG, Bebelis S, Pliangos C et al (2001) Electrochemical activation of catalysis: promotion, electrochemical promotion, and metal-support interactions. Kluwer Academic/Plenum, New York
46. Vayenas C, Brosda S, Pliangos C (2001) Rules and mathematical modeling of electrochemical and chemical promotion 1. Reaction classification and promotional rules. J Catal 203:329–350
47. Brosda S, Vayenas CG (2002) Rules and mathematical modeling of electrochemical and classical promotion 2. Modeling. J Catal 208:38–53
48. Brosda S, Vayenas C, Wei J (2006) Rules of chemical promotion. Appl Catal B Environ 68:109–124
49. Van Santen RA (1991) Chemical basis of metal catalyst promotion. Surf Sci 251(252):6–11
50. Ertl G, Lee SB, Weiss M (1982) Adsorption of nitrogen on potassium promoted Fe(111) and (100) surfaces. Surf Sci 114:527–545
51. Bécue T, Davis RJ, Garces JM (1998) Effect of cationic promoters on the kinetics of ammonia synthesis catalyzed by ruthenium supported on zeolite X. J Catal 179:129–137
52. Shekhah O, Ranke W, Schlogl R (2004) Styrene synthesis: in situ characterization and reactivity studies of unpromoted and potassium-promoted iron oxide model catalysts. J Catal 225:56–68
53. Zhu XM, Schön M, Bartmann U et al (2004) The dehydrogenation of ethylbenzene to styrene over a potassium-promoted iron oxide-based catalyst: a transient kinetic study. Appl Catal A Gen 266:99–108
54. Yentekakis IV, Lambert RM, Tikhov MS et al (1998) Promotion by sodium in emission control catalysis: a kinetic and spectroscopic study of the Pd- catalyzed reduction of NO by propene. J Catal 176:82–92
55. Yentekakis I, Konsolakis M, Lambert R et al (1999) Extraordinarily effective promotion by sodium in emission control catalysis: NO reduction by propene over Na-promoted Pt/γ-Al_2O_3. Appl Catal B Environ 22:123–133
56. Konsolakis M, Macleod N, Isaac J et al (2000) Strong promotion by Na of Pt/γ-Al_2O_3 catalysts operated under simulated exhaust conditions. J Catal 193:330–337
57. Pliangos C, Raptis C, Badas T et al (2000) Electrochemical promotion of a classically promoted Rh catalyst for the reduction of NO. Electrochim Acta 46:331–339
58. Ibrahim N, Poulidi D, Metcalfe IS (2013) The role of sodium surface species on electrochemical promotion of catalysis in a Pt/YSZ system: the case of ethylene oxidation. J Catal 303:100–109
59. Özbek MO, van Santen RA (2013) The mechanism of ethylene epoxidation catalysis. Catal Lett 143:131–141
60. Konsolakis M, Yentekakis IV (2001) The reduction of NO by propene over Ba-promoted Pt/γ-Al_2O_3 catalysts. J Catal 198:142–150. doi:10.1006/jcat.2000.3123
61. Hereijgers BPC, Weckhuysen BM (2009) Selective oxidation of methanol to hydrogen over gold catalysts promoted by alkaline-earth-metal and lanthanum oxides. ChemSusChem 2:743–748
62. Nagaraju P, Lingaiah N, Sai Prasad PS et al (2008) Preparation, characterization and catalytic properties of promoted vanadium phosphate catalysts. Catal Commun 9:2449–2454
63. Rodriguez P, Kwon Y, Koper MTM (2012) The promoting effect of adsorbed carbon monoxide on the oxidation of alcohols on a gold catalyst. Nat Chem 4:177–182

64. Tong YJ (2012) Unconventional promoters of catalytic activity in electrocatalysis. Chem Soc Rev 41:8195–8209
65. Schwab GM, Block J, Muller W, Schultze D (1957) Zur Natur der katalytischen Verstärker-Wirkung, Naturwissenschaften 44:582–584
66. Schwab GM, Block J, Schultze D (1958) Kontaktkatalytische Verstärkung durch dotierte Träger. Angew Chem 71:101–104
67. Tauster SJ, Fung SC, Garten RL (1978) Strong metal-support interactions. Group 8 noble metals supported on titanium dioxide. J Am Chem Soc 100:170–175
68. Lewera A, Timperman L, Roguska A, Alonso-Vante N (2011) Metal-support interactions between nanosized Pt and metal oxides (WO_3 and TiO_2) studied using X-ray photoelectron spectroscopy. J Phys Chem C 115:20153–20159
69. Jin M, Park J-N, Shon JK et al (2012) Low temperature CO oxidation over Pd catalysts supported on highly ordered mesoporous metal oxides. Catal Today 185:183–190
70. Metcalfe IS, Sundaresan S (1988) Oxygen transfer between metals and oxygen-ion conducting supports. AIChE J 34:195–208
71. Dow W-P, Huang T-J (1994) Effects of oxygen vacancy of yttria-stabilized zirconia support on carbon monoxide oxidation over copper catalyst. J Catal 147:322–332
72. Dow W-P, Wang Y-P, Huang T-J (1996) Yttria-stabilized zirconia supported copper oxide catalyst I. Effect of oxygen vacancy of support on copper oxide reduction. J Catal 160: 155–170
73. Dow W-P, Huang T-J (1996) Yttria-stabilized zirconia supported copper oxide catalyst II. Effect of oxygen vacancy of support on catalytic activity for CO oxidation. J Catal 160:171–182
74. Isaifan RJ, Dole HAE, Obeid E et al (2012) Metal-support interaction of Pt nanoparticles with ionically and non-ionically conductive supports for CO oxidation. Electrochem Solid State Lett 15:E14
75. Isaifan RJ, Baranova EA (2013) Catalytic electrooxidation of volatile organic compounds by oxygen-ion conducting ceramics in oxygen-free gas environment. Electrochem Commun 27:164–167
76. Park JB, Graciani J, Evans J et al (2009) High catalytic activity of $Au/CeO_x/TiO_2(110)$ controlled by the nature of the mixed-metal oxide at the nanometer level. Proc Natl Acad Sci U S A 106:4975–4980
77. Jiménez-Borja C, Matei F, Dorado F, Valverde JL (2012) Characterization of Pd catalyst-electrodes deposited on YSZ: influence of the preparation technique and the presence of a ceria interlayer. Appl Surf Sci 261:671–678
78. Dole HAE, Isaifan RJ, Sapountzi FM et al (2013) Low temperature toluene oxidation over Pt nanoparticles supported on yttria stabilized-zirconia. Catal Lett 143:996–1002
79. Toshima N (2010) Chapter 17: Inorganic nanoparticles for catalysis. In: Altavilla C, Ciliberto E (eds) Inorganic nanoparticles: synthesis, applications, and perspectives. CRC Press, Boca Raton, pp 475–505
80. Tauster SJ (1987) Strong metal-support interactions. Acc Chem Res 20:389–394
81. Vernoux P, Lizarraga L, Tsampas MN et al (2013) Ionically conducting ceramics as active catalyst supports. Chem Rev 113:8192–8260
82. Sato H (1977) Some theoretical aspects of solid electrolytes. In: Geller S (ed) Solid electrolytes. Springer, Berlin/Heidelberg, pp 3–39
83. Bagotsky VS (2006) Nonaqueous electrolytes. In: Fundamentals of electrochemistry, 2nd edn. Wiley, Hoboken, pp 127–137
84. Heyne L (1977) Electrochemistry of mixed ionic-electronic conductors. In: Geller S (ed) Solid electrolytes. Springer, Berlin/Heidelberg, pp 169–221
85. Stimming U, Hengyong T, Bagotsky VS (2006) Solid-state electrochemistry. In: Fundamentals of electrochemistry, 2nd edn. Wiley, Hoboken, pp 419–447
86. Chadwick AV, Savin SLP (2009) Ion-conducting nanocrystals: theory, methods, and applications. In: Kharton VV (ed) Solid state electrochemistry I: fundamentals, materials and their applications. Wiley-VCH Verlag GmbH/Betz-Druck GmbH, Weinheim, pp 79–132

87. Vernoux P, Guth M, Li X (2009) Ionically conducting ceramics as alternative catalyst supports. Electrochem Solid State Lett 12:E9–E11
88. Stoukides M, Vayenas C (1981) The effect of electrochemical oxygen pumping on the rate and selectivity of ethylene oxidation on polycrystalline. J Catal 70:137–146
89. Yentekakis IV, Vayenas CG (1988) The effect of electrochemical oxygen pumping on the steady-state and oscillatory behavior of CO oxidation on polycrystalline Pt. J Catal 111:170–188
90. Bebelis S, Vayenas CG (1989) Non-Faradaic electrochemical modification. J Catal 146:125–146
91. Cavalca CA, Larson G, Vayenas CG, Haller GL (1993) Electrochemical modification of CH_3OH oxidation selectivity and activity on a Pt single-pellet catalytic reactor. J Phys Chem 97:6115–6119
92. Neophytides SG, Vayenas CG (1995) TPD and cyclic voltammetric investigation of the origin of electrochemical promotion in catalysis. J Phys Chem 99:17063–17067
93. Pacchioni G, Illas F, Neophytides S, Vayenas CG (1996) Quantum-chemical study of electrochemical promotion in catalysis. J Phys Chem 100:16653–16661
94. Vayenas CG, Bebelis S (1999) Electrochemical promotion of heterogeneous catalysis. Catal Today 51:581–594
95. Vayenas C, Brosda S, Pliangos C (2003) The double-layer approach to promotion, electrocatalysis, electrochemical promotion, and metal–support interactions. J Catal 216:487–504
96. Piram A, Li X, Gaillard F et al (2005) Electrochemical promotion of environmental catalysis. Ionics 11:327–332
97. De Lucas-Consuegra A, Dorado F, Jiménez-Borja C, Valverde JL (2008) Electrochemical promotion of Pt impregnated catalyst for the treatment of automotive exhaust emissions. J Appl Electrochem 38:1151–1157
98. Toghan A, Rösken LM, Imbihl R (2010) The electrochemical promotion of ethylene oxidation at a Pt/YSZ catalyst. Chemphyschem 11:1452–1459
99. Pliangos C, Raptis C, Bolzonella I et al (2002) Electrochemical promotion of conventional and bipolar reactor configurations for NO reduction. Ionics 8:372–382
100. Tsiplakides D, Balomenou S (2009) Milestones and perspectives in electrochemically promoted catalysis. Catal Today 146:312–318
101. Vayenas CG, Ladas S, Bebelis S et al (1994) Electrochemical promotion in catalysis: non-Faradaic electrochemical modification of catalytic activity. Electrochim Acta 39:1849–1855
102. Vayenas CG, Yentekakis IV, Bebelis S, Neophytides SG (1995) In-situ controlled promotion of catalyst surfaces via solid electrolytes – the NEMCA effect. Phys Chem Chem Phys 99:1393–1401
103. Vayenas G, Bebelis SI (1997) Electrochemical promotion. Solid State Ion 94:267–277
104. Metcalfe I (2001) Electrochemical promotion of catalysis I: thermodynamic considerations. J Catal 199:247–258
105. Metcalfe I (2001) Electrochemical promotion of catalysis II: the role of a stable spillover species and prediction of reaction rate modification. J Catal 199:259–272
106. Katsaounis A (2008) Electrochemical promotion of catalysis (EPOC) perspectives for application to gas emissions treatment. Glob Nest J 10:226–236
107. Tsiplakides D, Balomenou S (2008) Electrochemical promoted catalysis: towards practical utilization. Chem Ind Chem Eng Q 14:97–105
108. Vayenas CG, Koutsodontis CG (2008) Non-Faradaic electrochemical activation of catalysis. J Chem Phys 128:182506
109. Anastasijevic NA (2009) NEMCA – from discovery to technology. Catal Today 146: 308–311
110. Imbihl R (2010) Electrochemical promotion of catalytic reactions. Prog Surf Sci 85:241–278
111. Katsaounis A (2010) Recent developments and trends in the electrochemical promotion of catalysis (EPOC). J Appl Electrochem 40:885–902
112. Garagounis I, Kyriakou V, Anagnostou C et al (2011) Solid electrolytes: applications in heterogeneous catalysis and chemical cogeneration. Indust Eng Chem Res 50:431–472

113. Vayenas CG (2011) Bridging electrochemistry and heterogeneous catalysis. J Solid State Electrochem 15:1425–1435
114. Vayenas CG (1993) Electrochemical activation of catalysed reactions. In: Joyner RW, van Santen RA (eds) Elementary reaction steps in heterogeneous catalysis, 398th edn. Springer, Dordrecht, pp 73–92
115. Foti G, Bolzonella I, Comninellis C (2003) Electrochemical promotion of catalysis. In: Vayenas CG, Conway BE, White RE (eds) Modern aspects of electrochemistry, 36th edn. Plenum Press, New York, pp 191–254
116. Lambert RM (2003) Electrochemical and chemical promotion by alkalis with metal films and nanoparticles. In: Wieckowski A, Savinova ER, Vayenas CG (eds) Catalysis and electrocatalysis at nanoparticle surfaces. Marcel Dekker, New York, pp 583–612
117. Vayenas CG, Pliangos C, Brosda S, Tsiplakides D (2003) Promotion, electrochemical promotion, and metal-support interactions: the unifying role of spillover. In: Wieckowski AER, Savinova ER, Vayenas CG (eds) Catalysis and electrocatalysis at nanoparticle surfaces. Marcel Dekker, New York, pp 667–744
118. Jiménez-Borja C, de Lucas-Consuegra A, Valverde JL et al (2012) One of the recent discoveries in catalysis: the phenomenon of electrochemical promotion. In: Taylor JC (ed) Advances in chemistry research, 14th edn. Nova, New York, pp 99–132
119. Skriver HL, Rosengaard NM (1992) Surface energy and work function of elemental metals. Phys Rev B 46:7157–7168
120. Nicole J, Tsiplakides D, Wodiunig S, Comninellis C (1997) Activation of catalyst for gas-phase combustion by electrochemical pretreatment. J Electrochem Soc 144:L312–L314
121. Vayenas CG, Bebelis S, Neophytides S (1988) Non-Faradaic electrochemical modification of catalytic activity. J Phys Chem 92:5083–5085
122. Koutsodontis C, Katsaounis A, Figueroa JC et al (2006) The effect of catalyst film thickness on the electrochemical promotion of ethylene oxidation on Pt. Top Catal 39:97–100
123. Yentekakis IV, Bebelis S (1992) Study of the NEMCA effect in a single-pellet catalytic reactor. J Catal 137:278–283
124. Brosda S, Badas T, Vayenas CG (2011) Study of the mechanism of the electrochemical promotion of Rh/YSZ catalysts for C_2H_4 oxidation via AC impedance spectroscopy. Top Catal 54:708–717
125. Varkaraki E, Nicole J, Plattner E et al (1995) Electrochemical promotion of IrO_2 catalyst for the gas phase combustion of ethylene. J Appl Electrochem 25:978–981
126. Nicole J, Comninellis C (1998) Electrochemical promotion of IrO_2 catalyst activity for the gas phase combustion of ethylene. J Appl Electrochem 28:223–226
127. Tsiplakides D, Nicole J, Vayenas CG, Comninellis C (1998) Work function and catalytic activity measurements of an IrO_2 film deposited on YSZ subjected to in situ electrochemical promotion. J Electrochem Soc 145:905–908
128. Kaloyannis AC, Pliangos CA, Tsiplakides DT et al (1995) Electrochemical promotion of catalyst surfaces deposited on ionic and mixed conductors. Ionics 1:414–420
129. Poulidi D, Castillo-del-Rio MA, Salar R et al (2003) Electrochemical promotion of catalysis using solid-state proton-conducting membranes. Solid State Ion 162–163:305–311
130. Poulidi D, Mather GC, Tabacaru CN et al (2009) Electrochemical promotion of a platinum catalyst supported on the high-temperature proton conductor $La_{0.99}Sr_{0.01}NbO_{4-\delta}$. Catal Today 146:279–284
131. Yentekakis IV, Moggridge G, Vayenas CG, Lambert RM (1994) In situ controlled promotion of catalyst surfaces via NEMCA: the effect of Na on the Pt-catalyzed CO qxidation. J Catal 146:292–305
132. Lambert RM, Harkness IR, Yentekakis IV, Vayenas CG (1995) Electrochemical promotion in emission control catalysis. Ionics 1:29–31
133. Dorado F, de Lucas-Consuegra A, Jiménez C, Valverde JL (2007) Influence of the reaction temperature on the electrochemical promoted catalytic behaviour of platinum impregnated catalysts for the reduction of nitrogen oxides under lean burn conditions. Appl Catal A Gen 321:86–92

134. Dorado F, de Lucas-Consuegra A, Vernoux P, Valverde JL (2007) Electrochemical promotion of platinum impregnated catalyst for the selective catalytic reduction of NO by propene in presence of oxygen. Appl Catal B Environ 73:42–50
135. De Lucas-Consuegra A, Dorado F, Valverde JL et al (2008) Electrochemical activation of Pt catalyst by potassium for low temperature CO deep oxidation. Catal Commun 9:17–20
136. Tsiplakides D, Neophytides SG, Enea O et al (1997) Nonfaradaic electrochemical modification of the catalytic activity of Pt-black electrodes deposited on nafion 117 solid polymer electrolytes. J Electrochem Soc 144:2072–2078
137. Marwood M, Vayenas CG (1998) Electrochemical promotion of a dispersed platinum catalyst. J Catal 178:429–440
138. Jiménez-Borja C, Delgado B, Díaz-Díaz LF et al (2012) Enhancing the combustion of natural gas by electrochemical promotion of catalysis. Electrochem Commun 23:9–12
139. Li N, Gaillard F (2009) Catalytic combustion of toluene over electrochemically promoted Ag catalyst. Appl Catal B Environ 88:152–159
140. Theleritis D, Souentie S, Siokou A et al (2012) Hydrogenation of CO_2 over Ru/YSZ electropromoted catalysts. ACS Catal 2:770–780
141. Wodiunig S, Bokeloh F, Nicole J, Comninellis C (1999) Electrochemical promotion of RuO_2 catalyst dispersed on an yttria-stabilized zirconia monolith. Electrochem Solid State Lett 2:281–283
142. Xia C, Hugentobler M, Li Y et al (2010) Electrochemical promotion of CO combustion over non-percolated Pt particles supported on YSZ using a novel bipolar configuration. Electrochem Commun 13:99–101
143. Xia C, Hugentobler M, Comninellis C, Harbich W (2010) Quantifying electrochemical promotion of induced bipolar Pt particles supported on YSZ. Electrochem Commun 12: 1551–1554
144. Papaioannou EI, Souentie S, Sapountzi FM et al (2010) The role of TiO_2 layers deposited on YSZ on the electrochemical promotion of C_2H_4 oxidation on Pt. J Appl Electrochem 40:1859–1865
145. Karoum R, Roche V, Pirovano C et al (2010) CGO-based electrochemical catalysts for low temperature combustion of propene. J Appl Electrochem 40:1867–1873
146. Souentie S, Lizarraga L, Papaioannou EI et al (2010) Permanent electrochemical promotion of C_3H_8 oxidation over thin sputtered Pt films. Electrochem Commun 12:1133–1135
147. Lizarraga L, Souentie S, Mazri L et al (2010) Investigation of the CO oxidation rate oscillations using electrochemical promotion of catalysis over sputtered-Pt films interfaced with YSZ. Electrochem Commun 12:1310–1313
148. Lizarraga L, Guth M, Billard A, Vernoux P (2010) Electrochemical catalysis for propane combustion using nanometric sputtered-deposited Pt films. Catal Today 157:61–65
149. Hammad A, Souentie S, Papaioannou EI et al (2011) Electrochemical promotion of the SO_2 oxidation over thin Pt films interfaced with YSZ in a monolithic electropromoted reactor. Appl Catal B Environ 103:336–342
150. Baranova EA, Thursfield A, Brosda S et al (2005) Electrochemical promotion of ethylene oxidation over Rh catalyst thin films sputtered on YSZ and TiO_2/YSZ supports. J Electrochem Soc 152:E40–E49
151. Balomenou S, Tsiplakides D, Katsaounis A et al (2004) Novel monolithic electrochemically promoted catalytic reactor for environmentally important reactions. Appl Catal B Environ 52:181–196
152. Balomenou S, Tsiplakides D, Katsaounis A et al (2006) Monolithic electrochemically promoted reactors: a step for the practical utilization of electrochemical promotion. Solid State Ion 177:2201–2204
153. Koutsodontis C, Hammad A, Lepage M et al (2008) Electrochemical promotion of NO reduction by C_2H_4 in excess O_2 using a monolithic electropromoted reactor and Pt–Rh sputtered electrodes. Top Catal 50:192–199
154. Roche V, Revel R, Vernoux P (2010) Electrochemical promotion of YSZ monolith honeycomb for deep oxidation of methane. Catal Commun 11:1076–1080

155. Dole HAE, Safady LF, Ntais S et al (2014) Improved catalytic reactor for electrochemical promotion of highly dispersed Ru nanoparticles with CeO_2 support. ECS Trans 61:65–74
156. Lintanf A (2008) Pt/YSZ electrochemical catalysts prepared by electrostatic spray deposition for selective catalytic reduction of NO by C_3H_6. Solid State Ion 178:1998–2008
157. Vayenas CG, Bebelis S, Yentekakis IV, Lintz H-G (1992) Non-Faradaic electrochemical modification of catalytic activity: a status report. Catal Today 11:303–442
158. Baranova EA, Thursfield A, Brosda S et al (2005) Electrochemically induced oscillations of C_2H_4 oxidation over thin sputtered Rh catalyst films. Catal Lett 105:15–21
159. Baranova EA, Fóti G, Jotterand H, Comninellis C (2007) Electrochemical modification of the catalytic activity of TiO_2/YSZ supported rhodium films. Top Catal 44:355–360
160. Constantinou I, Archonta D, Brosda S et al (2007) Electrochemical promotion of NO reduction by C_3H_6 on Rh catalyst-electrode films supported on YSZ and on dispersed Rh/YSZ catalysts. J Catal 251:400–409
161. Jiménez-Borja C, Dorado F, de L -Consuegra A et al (2011) Electrochemical promotion of CH_4 combustion over a Pd/CeO_2-YSZ catalyst. Fuel Cells 11:131–139
162. Kambolis A, Lizarraga L, Tsampas MN et al (2012) Electrochemical promotion of catalysis with highly dispersed Pt nanoparticles. Electrochem Commun 19:5–8
163. Marwood M (1997) Electrochemical promotion of electronically isolated Pt catalysts on stabilized zirconia. J Catal 168:538–542
164. Balomenou S, Pitselis G, Polydoros D et al (2000) Electrochemical promotion of Pd, Fe and distributed Pt. Solid State Ion 137:857–862
165. Poulidi D, Mather G, Metcalfe I (2007) Wireless electrochemical modification of catalytic activity on a mixed protonic–electronic conductor. Solid State Ion 178:675–680
166. Poulidi D, Thursfield A, Metcalfe IS (2007) Electrochemical promotion of catalysis controlled by chemical potential difference across a mixed ionic-electronic conducting ceramic membrane – an example of wireless NEMCA. Top Catal 44:435–449
167. Poulidi D, Metcalfe IS (2008) Comparative studies between classic and wireless electrochemical promotion of a Pt catalyst for ethylene oxidation. J Appl Electrochem 38: 1121–1126